Trimeric precursors in formation of Al magic clusters on a Si(111)-7 × 7 surface

Hongjun Liu,[1,2,*] Jyh-Pin Chou,[3] Run-Wei Li,[1,4] Ching-Ming Wei,[3,†] and Kazushi Miki[1,2,‡]

[1]*National Institute for Materials Science (NIMS), 1-1 Namiki, Tsukuba 305-0044, Japan*

[2]*Graduate School of Pure and Applied Sciences, University of Tsukuba, Tsukuba 305-8571, Japan*

[3]*Institute of Atomic and Molecular Sciences, Academia Sinica, Taipei 106, Taiwan, Republic of China*

[4]*Ningbo Institute of Material Technology and Engineering (NIMTE), Chinese Academy of Sciences (CAS), Ningbo, Zhejiang, 315201, People's Republic of China*

(Received 26 April 2010; revised manuscript received 25 October 2010; published 7 February 2011)

The formation process of Al magic clusters on the Si(111)-7 × 7 surface was investigated by means of a variable-temperature scanning tunneling microscope (STM) *in situ* and was interpreted using density-functional theory (DFT) calculations. At a growth temperature of 450 °C, Al atoms hopped among the corner, center, and T4 sites and also across the dimer rows on the Si(111)-7 × 7 surface. At low coverage below 0.08 ML, a single Al atom was adsorbed on the corner or center site. When the coverage was increased to 0.08 ML, Al dimers and trimers appeared, and Al magic clusters were also observed. However, no Al tetramers or pentamers were experimentally confirmed. Careful analysis of STM images suggests that Al trimers could be key precursors for the formation of Al magic clusters, and DFT calculations verified this interpretation. Total-energy calculation results using DFT reveal that this is due to the small energy gain from Al trimer to Al tetramer. These results are important for understanding the atomic structure and the formation mechanism of the magic clusters on the Si(111)-7 × 7 surface.

DOI: 10.1103/PhysRevB.83.075405 PACS number(s): 61.46.Bc, 81.16.Dn, 68.37.Ef, 68.43.Bc

I. INTRODUCTION

Surface nanostructures are immensely attractive to researchers because of their interesting and novel morphology and potential applications.[1] Fabrication of highly ordered nanostructures on special substrates is a fascinating challenge for material researchers. Also, self-organization on templates is considered an effective way to build highly ordered nanocluster arrays.[2] For instance, one- and two-dimensional nanostructures have been created by diffusion-controlled aggregation of adsorbates on surfaces.[3] However, it is difficult to obtain perfectly ordered nanocluster arrays both with a uniform size and with an identical spacing since the growth process is associated with many thermodynamic and kinetic uncertainties. Recently, surface-mediated magic clustering was employed as the building blocks for identical-sized nanostructures, and the results demonstrated that the fabrication of artificial cluster crystals is possible.[4–15] While the fabrication of precise surface nanostructures has made exciting progress, the formation mechanism for this kind of surface magic cluster is still poorly understood, partly because of the complexity of the process from formation to detection. Recent experiments using a variable-temperature scanning tunneling microscope (STM) have given an unprecedented view of epitaxial nucleation and island growth. It is possible to explain how atoms can aggregate into well-defined clusters by self-organization.[16] However, the identification of adsorption sites remains nontrivial since an STM measures only the local density of states near the Fermi level rather than the metallic atoms themselves, and first-principles calculations were employed to understand the adsorption sites.[17]

Since its successful preparation, Al magic cluster arrays on the Si(111)-7 × 7 surface have been regarded as a good template for constructing highly ordered, artificial nanostructures.[12] They can form large-scale perfect nanocluster arrays with identical cluster size and spacing, even up to the step edges,[6–8] which provide an ideal periodic template for constructing artificial nanostructures. Through STM images and first-principles calculations, Jia *et al.* provided the atomic model for Al_6Si_3 magic clusters.[6,7] Our previous studies reported the thermal stability of Al magic cluster arrays and the interaction between arrays.[13–15] It was found that the Al magic cluster arrays are stable up to 500 °C, transforming into a $(\sqrt{3} \times \sqrt{3})$-Al phase above 500 °C. From the activation energy of the Al magic cluster, it was concluded that Al atoms congregate to form the Al magic cluster arrays through a single-atom diffusion process, rather than through a cluster diffusion process. An attractive interaction was found between the Al magic clusters, which is responsible for the honeycomb structure. To date, several research results on the formation of the Al magic clusters have been reported. However, the specific formation process of the Al magic clusters remains unclear, and the evolution of the surface morphology is, at present, poorly understood.

In this work, the formation process of Al magic clusters was studied at the atomic scale using a STM as well as density-functional theory (DFT) calculations. The STM images were carefully observed and analyzed at 450 °C. The adsorption of Al atoms at various degrees of coverage was investigated and subsequently identified. Al trimers were observed during the formation process and are considered to be the key precursors for the formation of Al magic clusters. By combining this with our previous statistical work on the cluster density of the coverage dependence, the formation process is elucidated.

II. EXPERIMENTS AND CALCULATIONS

The experiments were performed using a JEOL 4500 variable-temperature STM combined with E-gun-type evaporators operated in an ultrahigh vacuum chamber (with base pressure 1×10^{-8} Pa). E-gun evaporation of Al with purity

of 99.99% was employed to grow the Al magic clusters in the STM chamber. The depositing flux rate was 0.03 ML per min (1 ML = one adsorbed atom per substrate atom). Samples were heated in the STM chamber by a direct current passing through them, and the temperature was monitored by means of an infrared pyrometer. A chemically etched tungsten tip was employed to collect STM images. Si(111) samples were cleaned briefly with a HF acid solution and degassed at about 600 °C for 12 h in the ultrahigh vacuum chamber. The clean Si(111)-7 × 7 surface with few defects was obtained by flashing several times to about 1150 °C and then very slowly decreasing the temperature. All STM images were recorded *in situ* at 450 °C, which is the depositing and annealing temperature. The STM was operated at a tunneling current of 50–100 pA.

During this investigation, the results of DFT (Refs. 18 and 19) calculations were employed to understand the formation process. Periodic DFT calculations were performed using the Vienna *ab-initio* simulation package (VASP) (Ref. 20) with projector-augmented-wave (PAW) pseudopotentials.[21] The exchange-correlation effects have been described within the generalized gradient approximation (GGA) through the Perdew-Burke-Ernzerhof (PBE) functional. Wave functions were represented using a plane-wave basis set with a kinetic energy cutoff of 300 eV. The supercell geometry used in this study is simulated by a repeating slab of four atomic bilayers and a vacuum region of ∼9 Å. The adsorbed Al atoms are accommodated on the reconstructed (7 × 7) surface containing 396 silicon atoms, and the dangling bonds on the unreconstructed surface are saturated by 49 hydrogen atoms. Brillouin-zone integration was approximated at the Γ point. In all the calculations, the top three atomic bilayers are fully relaxed, and the bottom bilayer is fixed at the bulk position. The geometry is optimized until the total energy is converged to 1×10^{-4} eV. In this work, the binding energy is defined as the total energy of the adsorbed system minus the total energy of the free Al atoms and the Si(111)-7 × 7 surface.

III. RESULTS AND DISCUSSION

At the growth temperature of 450 °C, Al atoms were deposited onto the Si(111)-7 × 7 surface with coverage of 0.12 ML, as shown in Fig. 1. Al atoms and magic clusters can be observed on the surface at the growth temperature. The large bright dots on the surface were identified as Al_6Si_3 magic clusters,[6–8] and the small bright dots were considered to be single Al atoms.[22,23] A sequence of images at 100-s intervals was observed at 450 °C to investigate the stability and movement of the Al magic clusters. In Fig. 1, the unit cells of the Si(111)-7 × 7 surface are indicated with black lines to show the position of Al atoms and magic clusters. The fixed position of five large bright dots outlined by a blue square at the lower left corner is used as a marker to show that these three images are in almost the same area. The number and position of Al magic clusters are noticeably the same in all three images. At the same time, through the unit cells marked with solid (yellow) and dashed (green) rings, it can be seen that the number and position of Al atoms are different in these

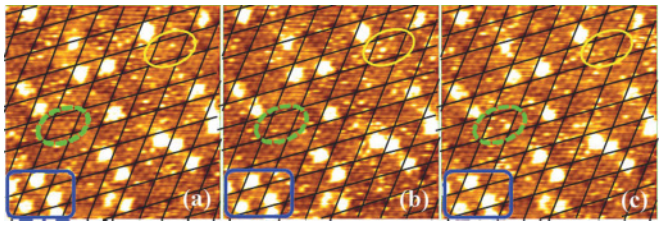

FIG. 1. (Color online) (a)–(c) are sequential empty-state STM images (at +2.0 V, 0.1 nA) of Al atoms on the Si(111)-7 × 7 surface after growth at 450 °C, which were extracted from one movie observed at 450 °C. The time interval is 100 s between two images. Al coverage is about 0.12 ML. The scanning size is 20.0 × 20.0 nm^2. The unit cells of the Si(111)-7 × 7 surface are indicated with black lines. The fixed structure outlined by a blue square is used as a marker to show that the three images are in the same area. Dashed (green) rings and solid (yellow) rings show the movement of Al atoms. The observed small and large bright dots are Al atoms and Al magic clusters, respectively.

figures, which demonstrates the rapid diffusion of Al atoms on the Si(111)-7 × 7 surface at the growth temperature. These results prove our previous supposition,[13] derived from the activation energy of Al magic cluster diffusion, in which we suggested that Al atom diffusion, rather than cluster diffusion, creates the Al magic cluster arrays. Once the Al magic cluster forms, it seldom decomposes or moves at the growth temperature. Thus, the formation process of the Al magic cluster is crucial for the formation of the Al magic cluster arrays. A better understanding of the formation process will lead to the synthesis of the perfect Al magic cluster array.

In order to study the evolution process of the Al magic cluster on the Si(111)-7 × 7 surface, high-resolution STM images were collected at Al coverages of 0.03, 0.08, and 0.27 ML at the growth temperature of 450 °C as shown in Figs. 2(a), 3(a), and 4(a), respectively. During measurement, the bias was fixed at 1.5 V because of the difficulty in setting the bias when the sample is being heated by a direct current passing through it. At Al coverage of 0.03 ML, which is fairly low, single Al atoms and some Al clusters were observed on the surface as shown in Fig. 2(a). In this image, single Al atoms that stayed at the corner and center sites are represented by bright dots marked with a red ring (denoted as s2) and without a ring (denoted as s1), respectively, while some Al atoms were adsorbed adjacent to other Al atoms inside the half-unit cell. DFT calculations were performed to understand the adsorption structure of single Al atoms. In this work, only the calculation results are employed to elucidate the STM observations. A detailed description of the DFT calculations and results will be published elsewhere.[24] Table I shows the

TABLE I. Calculated binding energies of Al atoms at different adsorption sites.

	Single Al atom			Al dimer		Al trimer	
Figure	2(b)	2(c)	2(d)	3(b)	3(c)	3(d)	3(e)
Binding energy per atom (eV)	−3.16	−3.14	−3.19	−3.58	−3.57	−3.66	−3.76

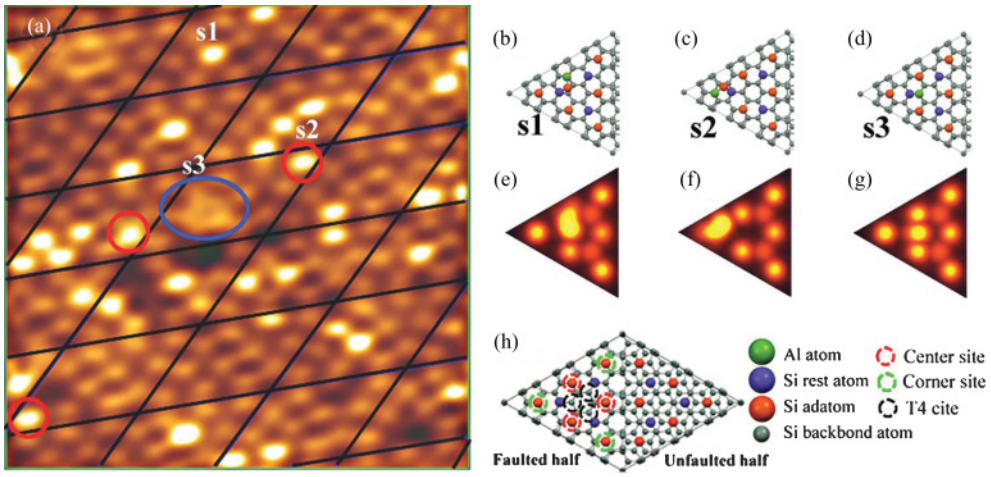

FIG. 2. (Color online) (a) Empty-state STM image of Al atoms on the Si(111)-7 × 7 surface observed at 450 °C. Sample bias is +1.5 V, tunneling current is 0.10 nA, scanning size is 9.0 × 9.0 nm^2, and Al coverage is 0.03 ML. The unit cells of the Si(111)-7 × 7 surface are indicated with black lines. Panels (b)–(d) show candidate adsorption models for a single Al atom on the faulted half-unit cell of the Si(111)-7 × 7 surface. Panels (e)–(g) show simulated STM images for the corresponding models (b)–(d). Panel (h) shows the model for the Si(111)-7 × 7 unit cell. In one half of the unit cell, six adatoms on the top layer form the triangle. The sites in the corner of the triangle and at the center of each edge of the triangle are defined as the corner and center sites, respectively, while the sites between the two center sites and above the Si atom on the second layer are defined as T4 sites. These three types of sites are common adsorption sites for adsorbates on the Si(111)-7 × 7 surface.

calculated binding energy of Al with different atom numbers (single Al atom, Al dimer, and Al trimer). For a single Al atom on an Al cluster, our previous work[15] showed that there is not much difference in adsorption site or in its probability between the two subunit cells of the Si(111)-7 × 7 surface: the faulted half and unfaulted half of the unit cell are shown in Fig. 2(h). Therefore, in this work, the binding energy and the simulated STM images on the faulted half of the unit cell will be presented. For single Al atom adsorption, the calculation results show that the configuration in Figs. 2(b) and 2(c) has lower binding energies of −3.16 and −3.14 eV, respectively. In these two configurations, an Al atom replaces a corner/center Si adatom and the repelled Si atom stays beside the Al atom. The corresponding simulated STM images [Figs. 2(e) and 2(f)] agree well with the observed STM patterns of s1 and s 2 in Fig. 2(a), respectively. Moreover, the calculation results show that the T4 adsorption site [Fig. 2(d)] has the lowest binding energy at −3.19 eV. However, in our observations, no corresponding pattern agreed with the simulated STM image of Fig. 2(g). Several studies have reported a "basin of attraction" in the half-unit cell of the Si(111)-7 × 7 surface.[4,17,25,26] The diffusion barriers within this basin are very low, and metal atoms, such as Na, Ga, K, Cu, Ag, and Au, can hop within the basin at the appropriate temperature. The calculated energy barrier for the Al atom within this basin is 0.36 eV, and therefore, it has the same behavior as that at the growth temperature of 450 °C, where Al atoms could freely diffuse within the basin on the Si(111)-7 × 7 surface. This diffusion is too fast to be observed by a STM. In the blue oval ring in Fig. 2(a), there is a cloudy zone (denoted as s3) in the half-unit cell, which is possibly explained by the diffusion of an Al atom among the three T4 sites in the half-unit cell.

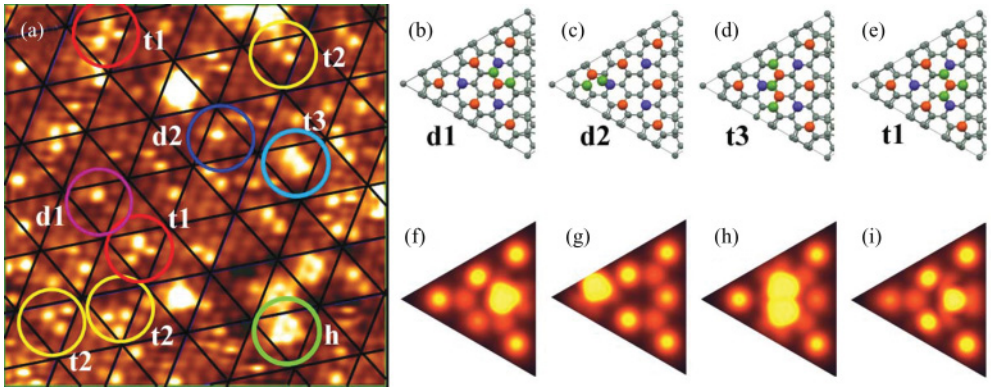

FIG. 3. (Color online) (a) Empty-state STM image of Al dimers and Al trimers on the Si(111)-7 × 7 surface observed at 450 °C. Sample bias is +1.5 V, tunneling current is 0.10 nA, scanning size is 15.0 × 15.0 nm^2, and Al coverage is 0.08 ML. Half-unit cells of the Si(111)-7 × 7 surface are indicated with black lines. Panels (b)–(e) show candidate adsorption models for Al dimers and Al trimers on the Si(111)-7 × 7 surface. Panels (f)–(i) are simulated STM images for the corresponding models (b)–(e), respectively.

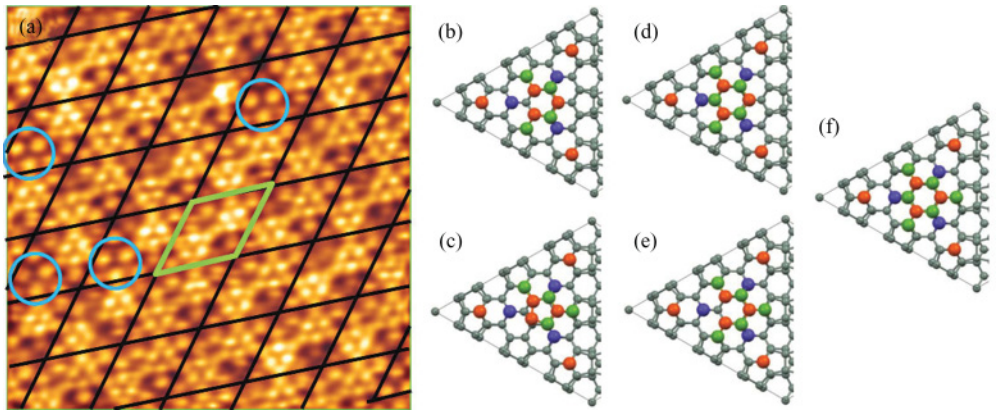

FIG. 4. (Color online) (a) Empty-state STM image of Al atoms on the Si(111)-7 × 7 surface observed at 450 °C. Sample bias is +1.5 V, tunneling current is 0.10 nA, scanning size is 13.3 × 13.3 nm^2, and Al coverage is 0.27 ML. The unit cells of the Si(111)-7 × 7 surface are indicated with black lines. Panels (b) and (c) show the adsorption models for an Al tetramer, panels (d) and (e) show those for an Al pentamer, and panel (f) is the model for an Al hexamer.

When the coverage increased to 0.08 ML, as shown in Fig. 3(a), several large clusters were observed. The bright triangular cluster (denoted as h and marked with a green ring) is assigned to the Al_6Si_3 magic cluster.[6–8] Two kinds of triangular bright spots were observed in the STM image: one is the occupation at the three center sites (denoted as t1 and marked with red rings) and the other is the occupation of the two center sites and one corner site (denoted as t2 and marked with yellow rings). To analyze these features, we calculated various possible configurations of two and three Al atoms on the Si(111)-7 × 7 surface. The results for the single Al atom reveal its preference for adsorption at the corner, center, and T4 sites on the Si(111)-7 × 7 surface; thus, the adsorption configuration for two and three Al atoms could be regarded as the combination of these three types of favorable sites. For two Al atoms, we calculated 10 configurations with different combinations, and the two lowest binding energies are listed in Table I. The calculation results reveal that stable configuration for two Al atoms is one atom at the center site and the other at the T4 site [Fig. 3(b)], which has an adsorption energy of −3.58 eV per atom. The other stable configuration is one Al atom at a corner site and the other at the T4 site [Fig. 3(c)], which is only 0.01 eV higher than the configuration in Fig. 3(b). For adsorption of three Al atoms, 19 configurations were considered, and the two lowest binding energies are also listed in Table I. One stable configuration is one Al atom at the center site and two atoms at the T4 site as shown in Fig. 3(d). The other configuration is two Al atoms at the center site and one at the T4 site as shown in Fig. 3(e). The corresponding simulated STM images of these stable dimer and trimer configurations are indicated in Figs. 3(f)–3(i). By comparing the simulated STM images with the experimental results of Fig. 2(a), it is found that there are no stable Al dimer and trimer adsorption configurations for the case of low Al coverage of around 0.03 ML, although it seems that there are some single Al atoms inside the same cell. Thus, we concluded that a single Al atom could be adsorbed at one of the stable sites on the Si(111)-7 × 7 surface, independently, even if the site is adjacent to other Al atoms, and several independently adsorbed single Al atoms could be observed at the same half-unit cell and could be regarded as a cluster.

Comparing the simulated STM images in Figs. 3(f)–3(i) with the experimental results of Fig. 3(a), Al dimers and trimers are recognized in the observed STM images. The bright dots denoted as d1 and d2 (marked with magenta and blue rings, respectively) are assigned to the Al dimer configuration of Figs. 3(b) and 3(c). The pattern t1 in Fig. 3(a) agrees with the simulated STM image of Fig. 3(i), so that t1 has the configuration of Fig. 3(e), which is that of the most stable trimer. However, t2 has no identical simulated STM image, so we conclude that t2 is not a stable trimer but instead is a combination of three stably adsorbed single Al atoms. The pattern t3, marked with the cyan ring in Fig. 3(a), corresponds to the simulated STM image of Fig. 3(h), the configuration of which is shown in Fig. 3(d). These trimers were often observed in the nearly perfect Al magic cluster array at the growth temperature of 450 °C. The trimers appear to be defect structures in the Al magic cluster array at a higher coverage of 0.27 ML [three bright dots marked with cyan rings in Fig. 4(a)] caused by a deficiency of Al atoms. This also provides evidence of the stability of the Al trimers as precursors. Al tetramers and pentamers were not experimentally confirmed during the evolution process of the Al hexamer (Al_6Si_3 magic cluster) on the Si(111)-7 × 7 surface. Comparing the configurations of the Al trimer [Figs. 3(d) and 3(e)] with the Al_6Si_3 magic cluster [Fig. 4(f)], we find that both of these trimers are part of the Al_6Si_3 magic cluster. Therefore, we believed that the Al trimer could be the precursor for the formation process of the Al magic cluster.

The calculated binding energies of the Al tetramer [Figs. 4(b) and 4(c)], pentamer [Figs. 4(d) and 4(e)], and hexamer [Fig. 4(f)] are presented in Table II. According to

TABLE II. Calculated binding energies of Al tetramer, pentamer, and hexamer structure in different adsorption configurations.

	Tetramer		Pentamer		Hexamer
Figure	4(b)	4(c)	4(d)	4(e)	4(f)
Binding energy per atom (eV)	−3.51	−3.65	−3.87	−3.86	−4.10

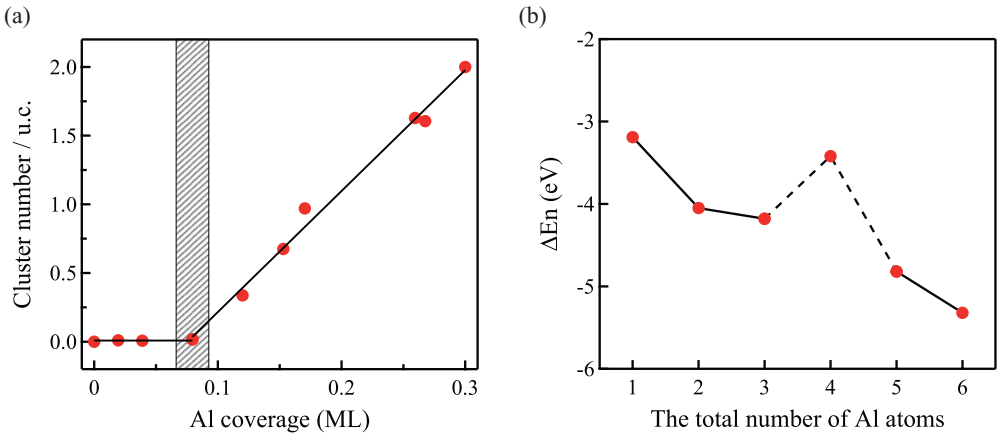

FIG. 5. (Color online) (a) Average cluster density per unit cell as a function of the Al coverage, observed with a STM at 450 °C. (b) Calculated incorporation energy as a function of the Al coverage, defined as the energy reduction of the Al-Si system when one more Al atom is incorporated into the Al_{n-1} cluster to form the Al_n cluster, $\Delta E_n = E_n - E_{n-1}$. Here, E_n is the total binding energy per half unit of the Si(111)-7 × 7 surface.

the binding energies listed in Tables I and II, the incorporation energy ΔE_n, defined as the energy reduction of the Al-Si system when one more Al atom is incorporated into the Al_{n-1} cluster to form an Al_n cluster for the complete formation process of Al_n $(n = 1 - 6)$ on the Si(111)-7 × 7 surface, is calculated as $\Delta E_n = E_n - E_{n-1}$, where E_n is the total binding energy and is presented in Table III. Figure 5(b) is the calculated incorporation-energy (ΔE_n) curve for the formation process of the Al magic cluster as each additional Al atom is incorporated into the cluster Al_{n-1}. The curve shows that the magnitude of incorporation energy (or energy gain) for Al tetramer is smaller than that of Al trimer, which means that $-\Delta E_4 < -\Delta E_3 (|E_4 - E_3| < |E_3 - E_2|)$. Therefore, the Al tetramer cluster [Figs. 4(b) and 4(c)] cannot form, but the Al trimer cluster plus the single Al monomer should remain, which is why no tetramer was observed during our experiments. Only when the density of Al atoms is high enough to reduce the increasing chemical potential will two Al atoms have to join the Al trimers together to form the Al pentamer. At the same time, another Al atom could quickly join the Al pentamer cluster to form the stable Al_6Si_3 magic cluster (hexamer) because the density of Al atoms is high at that time. We speculate that the process from Al pentamer to Al hexamer is so quick that it cannot be observed with a STM, which could be the reason why no pentamer was observed during our experiments. Thus, there could be a critical value of Al coverage during the formation process of the Al magic cluster array. In that case, if Al coverage is below a certain critical coverage, the diffusing Al atoms cannot be accommodated by the Al trimers to create the magic clusters. This agrees with our previous statistical work[15] [Fig. 5(a)] on the formation of Al magic clusters and the results reported by Kotlyar *et al.*[8]

TABLE III. Calculated incorporation energy as a function of the Al coverage, defined as the energy reduction of the Al-Si system when one more Al atom is incorporated into the Al_{n-1} cluster to form the Al_n cluster, $\Delta E_n = E_n - E_{n-1}$. Here, E_n is the total binding energy per half unit cell of the Si(111)-7 × 7 surface.

Number of Al atoms n	1	2	3	4	5	6
E_n (eV)	−3.19	−4.05	−4.18	−3.42	−4.82	−5.32

Accordingly, we understand the formation process of the Al magic cluster as follows: Single Al atoms prefer adsorption on the corner or the center sites, replacing the Si adatoms at the original position. As the coverage increases, the Al trimer forms, building the framework for the Al magic cluster. When the density of Al atoms is high enough, near 0.08 ML, an additional three Al atoms join the Al trimers to form the Al_6Si_3 clusters [Fig. 4(f)]. The formation of the Al_6Si_3 magic clusters removes three dangling bonds from the Si adatoms and three dangling bonds from the rest of the adatoms. The Al atoms and Si atoms form chemical bonds, and there is no dangling bond in the cluster, which makes the cluster very stable even at 500 °C. The stability of Al_6Si_3 also prevents the formation of even bigger clusters.

IV. SUMMARY

Combining STM observations with DFT calculations, the adsorption structures of Al_n $(n = 1 - 6)$ on the Si(111)-7 × 7 surface have been identified. Most of the DFT calculations agree well with the STM observations. The Al trimer is the key precursor state for the formation process of the Al magic cluster, and the formation process has been elucidated. At 450 °C, Al atoms hop among the corner, center, and T4 sites on the Si(111)-7 × 7 surface. At low coverage below 0.08 ML, single Al atoms adsorb independently at the corner or center sites and repel Si atoms from the original position. When the coverage increases to 0.08 ML, the Al dimers and trimers form, and then the other three Al atoms join the trimer and eventually form the complete Al_6Si_3 magic cluster. These results offer a comprehensive understanding of the atomic structure of the Al_6Si_3 magic cluster and provide insight into the formation mechanism of Al magic cluster arrays. We are also aware of the possibilities of special statistical effects, which could explain the critical value of 0.08 ML beyond which the Al_6Si_3 magic cluster density increases linearly with the coverage and which

would indicate that normal thermal equilibrium condition can be assumed.

No tetramer was observed during our STM observations. Based on the calculated binding energies from DFT, the energy gain for the Al tetramer is smaller than that for the Al trimer, which means that the tetramer cluster cannot form but the Al trimer cluster and single Al monomer should remain. This is why no tetramer was observed during our experiments. However, questions remain about the formation process from the Al trimer, the key precursor state, to the Al magic cluster. For example, what are the exact processes from Al trimer to tetramer, pentamer, and, finally, Al magic cluster? We anticipate that if two Al atoms join into the Al trimer together to form the Al pentamer, this process will be possible. As the energy gain from pentamer to hexamer is the largest (see Table III), it would be very easy to form a hexamer (Al_6Si_3 magic cluster) from a pentamer. Detailed studies of these dynamics are currently under way and will be published in the future.

ACKNOWLEDGMENTS

We thank Dr. James Owen for his comments and revision of the manuscript. We thank Dr. Canhua Liu for fruitful discussion. This research was partially supported by the Ministry of Education, Culture, Sports, Science and Technology (MEXT) of Japan, Grant-in-Aid for Scientific Research, the Iketani Science and Technology Foundation, and the A3 Foresight Program of the Japanese Society for the Promotion of Science. This work was also supported in part by the National Science Council of Taiwan under Grants No. NSC96-2628-M-001-006-MY3 and No. NSC99-2112-M-034-MY3.

*liu.hongjun@nims.go.jp
†cmw@phys.sinica.edu.tw
‡miki.kazushi@nims.go.jp

[1] H. Brune, Surf. Sci. Rep. **31**, 125 (1998).
[2] J. V. Barth, G. Costantini, and K. Kern, Nature (London) **437**, 671 (2005).
[3] H. Roder, E. Hahn, H. Brune, J. P. Bucher, and K. Kern, Nature (London) **366**, 141 (1993).
[4] L. Vitali, M. G. Ramsey, and F. P. Netzer, Phys. Rev. Lett. **83**, 316 (1999).
[5] M. Y. Lai and Y. L. Wang, Phys. Rev. B **64**, 241404 (2001).
[6] J. F. Jia, J. Z. Wang, X. Liu, Q. K. Xue, Z. Q. Li, Y. Kawazoe, and S. B. Zhang, Appl. Phys. Lett. **80**, 3186 (2002).
[7] J. F. Jia, X. Liu, J. Z. Wang, J. L. Li, X. S. Wang, Q. K. Xue, Z. Q. Li, Z. Y. Zhang, and S. B. Zhang, Phys. Rev. B **66**, 165412 (2002).
[8] V. G. Kotlyar, A. V. Zotov, A. A. Saranin, T. V. Kasyanova, M. A. Cherevik, I. V. Pisarenko, and V. G. Lifshits, Phys. Rev. B **66**, 165401 (2002).
[9] J. L. Li, J. F. Jia, X. J. Liang, X. Liu, J. Z. Wang, Q. K. Xue, Z. Q. Li, J. S. Tse, Z. Y. Zhang, and S. B. Zhang, Phys. Rev. Lett. **88**, 066101 (2002).
[10] J. F. Jia, J. Z. Wang, X. Liu, X. S. Wang, Q. K. Xue, Z. Q. Li, and S. B. Zhang, Nanotechnology **13**, 736 (2002).
[11] S. C. Li, J. F. Jia, R. F. Dou, Q. K. Xue, I. G. Batyrev, and S. B. Zhang, Phys. Rev. Lett. **93**, 116103 (2004).
[12] M. H. Pan, H. Liu, J. Z. Wang, J. F. Jia, Q. K. Xue, J. L. Li, S. Y. Qin, U. M. Mirsaidov, X. R. Wang, J. T. Markert, Z. Zhang, and C. K. Shih, Nano Lett. **5**, 87 (2005).
[13] R. W. Li, J. H. G. Owen, S. Kusano, and K. Miki, Appl. Phys. Lett. **89**, 073116 (2006).
[14] R. W. Li, S. Kusano, J. H. G. Owen, and K. Miki, Nanotechnology **17**, 2018 (2006).
[15] R. W. Li, H. J. Liu, J. H. G. Owen, Y. Wakayama, K. Miki, and H. W. Yeom, Phys. Rev. B **76**, 075418 (2007).
[16] C. J. Chen, *Introduction to Scanning Tunneling Microscopy*, 1st ed. (Oxford University Press, New York, Oxford, 1993).
[17] C. Zhang, G. Chen, K. Wang, H. W. Yang, T. Su, C. T. Chan, M. M. T. Loy, and X. D. Xiao, Phys. Rev. Lett. **94**, 176104 (2005).
[18] P. Hohenberg and W. Kohn, Phys. Rev. **136**, B864 (1964).
[19] W. Kohn and L. J. Sham, Phys. Rev. **140**, A1133 (1965).
[20] G. Kresse and J. Hafner, Phys. Rev. B **47**, 558 (1993).
[21] G. Kresse and D. Joubert, Phys. Rev. B **59**, 1758 (1999).
[22] H. Uchida, T. Kuroda, F. B. Mohamad, J. Kim, K. Kashiwagi, and K. Nishimura, Phys. Stat. Sol. B **241**, 1665 (2004).
[23] H. Uchida, T. Kuroda, F. B. Mohamad, J. Y. Kim, K. Nishimura, and M. Inoue, Surf. Sci. **566-568**, 197 (2004).
[24] J. Chou and C. M. Wei (unpublished).
[25] K. H. Wu, Y. Fujikawa, T. Nagao, Y. Hasegawa, K. S. Nakayama, Q. K. Xue, E. G. Wang, T. Briere, V. Kumar, Y. Kawazoe, S. B. Zhang, and T. Sakurai, Phys. Rev. Lett. **91**, 126101 (2003).
[26] K. Cho and E. Kaxiras, Surf. Sci. **396**, L261 (1998).